Proceedings of the 1st International Symposium on Steel Science (IS^3–2007)
The Iron and Steel Institute of Japan, 2007

The Nature, Mechanism and Properties of Strong Bainite

H. K. D. H. Bhadeshia

University of Cambridge, Materials Science and Metallurgy, U. K.
Graduate Institute of Ferrous Technology, POSTECH, S. Korea

Abstract: : Consistent with the wishes of the Conference Organisers, the basic theory of the bainite reaction including the crystallographic, thermodynamic and kinetic framework is described, together with the development of fine bainite and its properties.

1. INTRODUCTION

The description of a phase in a system which can decompose into many products is incomplete when based on isolated observations of that phase. It is necessary therefore to describe bainite in the context of the other solid–state transformations typical in steel. My remit also includes "superbainite" (an incredibly fine structure), and a request to outline the future of tough and ductile bainite. Ashby [1] in 1993 made a forecast of what he called the *relative importance* of materials, Fig. 1. He noted that "the rate of development of metals and alloys is now slow and demand for steel and cast iron has actually fallen". On these limited observations he predicted a huge decline in the relative importance of metals (Fig. 1). The estimate was so wrong, that it illustrates the futility of making forecasts. Steel production has never been higher than today (2007). I will refrain therefore from speculating about the future.

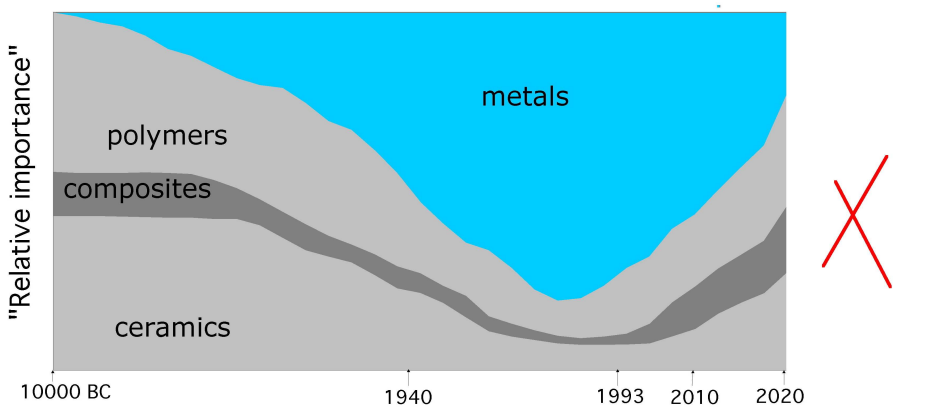

Figure 1: This is the incorrect forecast made in 1993 of the trend in the importance of materials. Adapted from [1].

2. THERMODYNAMICS

There is a change in the chemical composition of the austenite when it partly decomposes into ferrite. In contrast, the formation of a ferrite nucleus hardly affects the composition of the remaining austenite. The calculation of the free energy change for nucleation takes this difference into account. The free energy change for the formation of a mole of ferrite nuclei of composition x^α is given by ΔG_3, Fig. 2a [2, 3].

The greatest reduction in free energy during nucleation is obtained if the composition of the ferrite nucleus is set to a value x_m, given by a tangent to the ferrite free energy curve which is parallel to the tangent to the austenite free energy curve at $\overline{x}$, as shown in Fig. 2a. This maximum possible free energy change for nucleation is designated ΔG_m.

There is simplification when the transformation occurs without composition change (Fig. 2b). The change $\Delta G^{\gamma\alpha}$ is the vertical distance between the austenite and ferrite free energy curves at the composition of interest.

We shall henceforth use ΔG_m for the case where nucleation occurs by a paraequilibrium mechanism and $\Delta G^{\gamma\alpha}$ for cases where there is no change in composition on transformation.

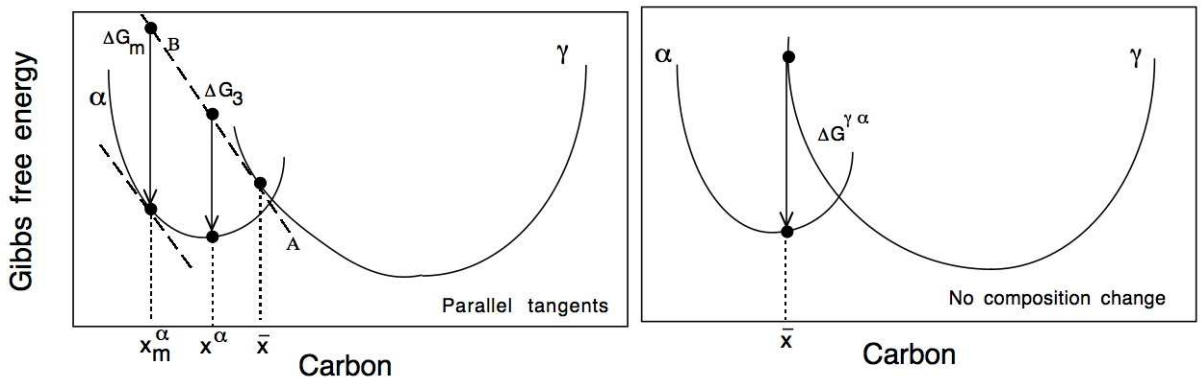

Figure 2: Free energy diagrams illustrating (a) the chemical free energy changes during the nucleation and (b) the growth of bainitic–ferrite from austenite of composition $\overline{x}$.

3. TRANSFORMATION–START TEMPERATURE

It is a common observation that the Widmanstätten ferrite–start (W_S) and bainite–start (B_S) temperatures are more sensitive to the steel composition than is the Ae_3 equilibrium–temperature. The influence of solutes on the nucleation of Widmanstätten ferrite and bainite is more than just thermodynamic, Fig. 3.

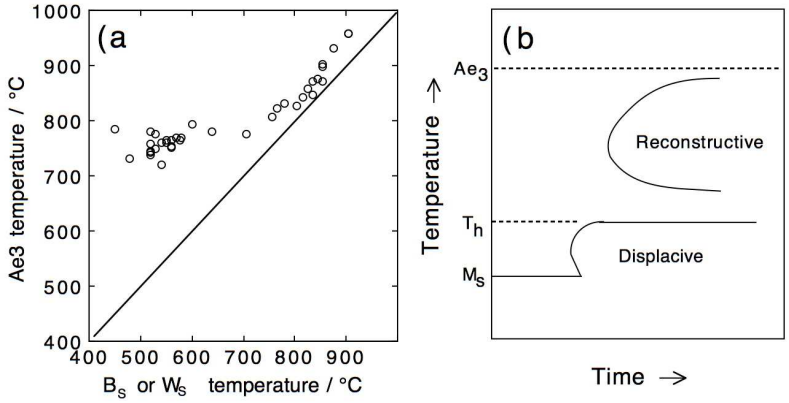

Figure 3: (a) Variation of the Widmanstätten ferrite–start and bainite–start temperatures as a function of the Ae_3 temperature [4]. (b) Schematic TTT diagram illustrating the two C–curves and the T_h temperature, which can be W_S or B_S depending on the prevailing thermodynamic conditions.

Some clues to this behaviour come from studies of time–temperature–transformation diagrams, which consist essentially of two C–curves. The lower C–curve has a characteristic flat top at a temperature T_h, which is the highest temperature at which ferrite can form by displacive transformation, Fig. 3. The transformation product at T_h may be Widmanstätten ferrite or bainite.

The driving force ΔG_m available for nucleation at T_h, is plotted in Fig. 4a, where each point comes from a different steel. The transformation product at T_h can be Widmanstätten ferrite or bainite, but it is found that there is no need to distinguish between these phases for the purposes of nucleation. The same nucleus can develop into either phase depending on the prevailing thermodynamic conditions. The analysis proves that carbon must partition during the nucleation stage to provide the free energy required for nucleation. Diffusionless nucleation is not viable since it would in some cases lead to an increase in the free energy, Fig. 4b.

The plots in Fig. 4 are generated using data from diverse steels. Fig. 4a represents the free energy change ΔG_m at the temperature T_h where displacive transformation first occurs. The free energy change can be calculated from readily available thermodynamic data. It follows that Fig. 4a can be used to estimate T_h for any steel. The equation fitted to the data in Fig. 4a is [2–4]:

$$G_N = C_1(T - 273.18) - C_2 \qquad \mathrm{J\,mol^{-1}} \tag{1}$$

where C_1 and C_2 are fitting constants for the illustrated temperature range. The linear relation between G_N and T is termed a *universal nucleation function*, because it defines the minimum driving force necessary to achieve a perceptible nucleation rate for Widmanstätten ferrite or bainite in any steel.

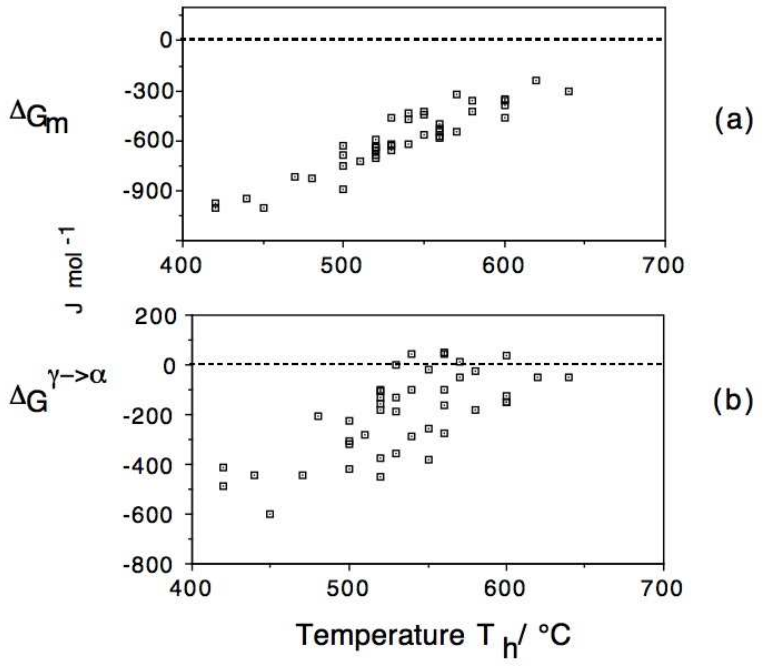

Figure 4: The free energy change necessary in order to obtain a detectable degree of transformation. Each point represents a different steel and there is no distinction made between Widmanstätten ferrite or bainite. (a) Calculated assuming the partitioning of carbon during nucleation. (b) Calculated assuming that there is no change in composition during nucleation. After [2, 3].

3.1 Evolution of the Nucleus

The nucleus is identical for Widmanstätten ferrite and for bainite; the transformations are distinguished by their growth mechanisms. But what determines whether the nucleus evolves into bainite or Widmanstätten ferrite?

The answer is straightforward. If diffusionless growth cannot be sustained at T_h then the nucleus develops into Widmanstätten ferrite so that T_h is identified with W_S. A larger undercooling is necessary before bainite can be stimulated. If, however, the driving force at T_h is sufficient to account for diffusionless growth, then $T_h = B_S$ and Widmanstätten ferrite does not form at all.

It follows that Widmanstätten ferrite forms below the Ae_3 temperature when:

$$\Delta G^{\gamma\rightarrow\gamma'+\alpha} < -G_{SW} \qquad \text{and} \qquad \Delta G_m < G_N \tag{2}$$

where G_{SW} is the stored energy of Widmanstätten ferrite (about 50 $\mathrm{J\,mol^{-1}}$). $\Delta G^{\gamma\rightarrow\gamma'+\alpha}$ is the free energy change associated with the paraequilibrium growth of Widmanstätten ferrite [5]. The first of these conditions ensures that the chemical free energy change exceeds the stored energy of the Widmanstätten ferrite, and the second that there is a detectable nucleation rate.

Bainite is expected below the T_0' temperature when:

$$\Delta G^{\gamma\alpha} < -G_{SB} \qquad \text{and} \qquad \Delta G_m < G_N \tag{3}$$

where G_{SB} is the stored energy of bainite (about 400 $\mathrm{J\,mol^{-1}}$). The universal function, when used with these conditions, allows the calculation of the Widmanstätten ferrite–start and bainite–start temperatures from a knowledge of thermodynamics alone.

In this scheme, carbon is partitioned during nucleation but in the case of bainite, not during growth which is diffusionless. There is no inconsistency in this concept since a greater fraction of the free energy becomes available as the particle surface to volume ratio, and hence the influence of interfacial energy, decreases.

4. MECHANISM OF NUCLEATION

The universal function G_N was originally derived by fitting to experimental data over the temperature range 400–650°C [2, 4] and has been demonstrated more recently for high–carbon steels [11]. It is nevertheless empirical and requires some justification for the linear dependence of G_N on T_h (Fig. 4) before it can be extrapolated to explore low transformation temperatures and address the question about the minimum temperature at which bainite can be obtained.

Classical nucleation theory involving heterophase fluctuations is not appropriate for bainite [3] given that thermal activation is in short supply. Furthermore, it leads to a relationship between the chemical driving force ΔG_{CHEM} and the activation energy G^* for nucleation as

$$G* \propto \Delta G_{CHEM}^{-2} \tag{4}$$

which cannot explain the proportionality between G_N and T_h [3].

One mechanism in which the barrier to nucleation becomes sufficiently small involves the spontaneous dissociation of specific dislocation defects in the parent phase [12, 13]. The dislocations are glissile so the mechanism does not require diffusion. The only barrier is the resistance to the glide of the dislocations. The nucleation event cannot occur until the undercooling is sufficient to support the faulting and strains associated with the dissociation process that leads to the creation of the new crystal structure.

The free energy per unit area of fault plane is:

$$G_F = n_P \rho_A (\Delta G_{CHEM} + G_{STRAIN}) + 2\sigma_{\alpha\gamma}\{n_P\} \tag{5}$$

where n_P is the number of close–packed planes participating in the faulting process, ρ_A is the spacing of the close–packed planes on which the faulting is assumed to occur. The fault energy can become negative when the austenite becomes metastable.

For a fault bounded by an array of n_P dislocations each with a Burgers vector of magnitude b, the force required to move a unit length of dislocation array is $n_P \tau_o b$. τ_o is the shear resistance of the lattice to the motion of the dislocations. G_F provides the opposing stress via the chemical free energy change ΔG_{CHEM}; the physical origin of this stress is the fault energy which becomes negative so that the partial dislocations bounding the fault are repelled. The defect becomes unstable, *i.e.,* nucleation occurs, when

$$G_F = -n_P \tau_o b \tag{6}$$

Take the energy barrier between adjacent equilibrium positions of a dislocation to be G_o^*. An applied shear stress τ has the effect of reducing the height of this barrier [14, 15]:

$$G^* = G_o^* - (\tau - \tau_\mu) v^* \tag{7}$$

where v^* is an activation volume and τ_μ is the temperature independent resistance to dislocation motion. In the context of nucleation, the stress τ is not externally applied but comes from the chemical driving force. On combining the last three equations we obtain [13]:

$$G^* = G_o^* + \left[\tau_\mu + \frac{\rho_A}{b} G_{STRAIN} + \frac{2\sigma}{n_P b}\right] v^* + \frac{\rho_A v^*}{b} \Delta G_{CHEM} \tag{8}$$

It follows that with this model of nucleation the activation energy G^* will decrease *linearly* as the magnitude of the driving force ΔG_{CHEM} increases. This direct proportionality contrasts with the inverse square relationship of classical theory.

The nucleation rate I_V will have a temperature dependence due to the activation energy:

$$I_V \propto \nu \exp\{-G^*/RT\} \tag{9}$$

where ν is an attempt frequency. It follows that

$$-G^* \propto \beta T \qquad \text{where} \qquad \beta = R \ln\{I_V/\nu\} \tag{10}$$

We now assume that there is a specific nucleation rate at T_h, irrespective of the type of steel, in which case β is a constant, negative in value since the attempt frequency should be larger than the actual rate. This gives the interesting result that

$$G_N \propto \beta T \tag{11}$$

which is precisely the relationship observed experimentally, Fig. 4a. This is evidence for nucleation by the dissociation of dislocations with the activation energy proportional to the driving force, as opposed to the inverse square relationship predicted by classical theory. The activation energy G^* in this model comes from the resistance of the lattice to the motion of dislocations.

Nucleation corresponds to a point where the slow, thermally activated migration of glissile partial dislocations gives way to rapid, breakaway dissociation. This is why it is possible to observe two sets of transformation units, the first consisting of very fine embryo platelets below the size of the operational nucleus, and the second the size corresponding to the rapid growth to the final size. Intermediate sizes are rarely observed because the time period for the second stage is expected to be much smaller than that for the first. Figure 5 shows that in addition to the fully growth sub–units (a few micrometers in length), there is another population of much smaller (submicron) particles which represent the embryos at a point in their evolution prior to breakaway.

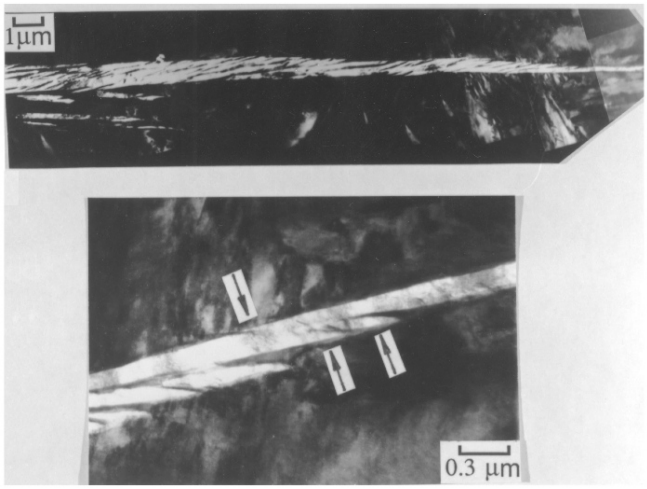

Figure 5: Transmission electron micrograph of a sheaf of bainite in a partially transformed sample. A region near the tip of the sheaf in (a) is enlarged in (b). The arrows in (b) indicate possible sub–operational embryos which are much smaller than the fully grown sub–units seen in (a). After [16]

5. MECHANISM OF GROWTH

In the absence of carbide precipitation, the bainite reaction stops when the driving force for diffusionless growth is exhausted. This and other observations lead to the conclusion that the individual platelets growth without diffusion, and that the carbon subsequently partitions into the residual austenite [17–21]

The scale of individual plates of bainitic ferrite is too small to be resolved adequately using optical microscopy, which is capable only of revealing clusters of plates. Using higher resolution techniques such as photoemission electron microscopy it has been possible to study directly the progress of the bainite reaction. Not surprisingly, the lengthening of individual bainite platelets has been found to occur at a rate which is much faster than expected from a diffusion–controlled process. The growth rate is nevertheless much smaller than that of martensite, because of the plasticity associated with the accommodation of the invariant–plane strain shape change. The platelets tend to grow at a constant rate but are usually stifled before they can traverse the austenite grain.

The complete scheme which describes the atomic mechanisms of solid–state transformations from austenite has been elaborated elsewhere [3, 18], but Table 1 summarises the essential details for Widmanstätten ferrite, bainite and martensite. These are some of the details which permit alloy design.

Table 1: Mechanisms of Displacive Transformations

Martensite α'	Bainite α_b	Widmanstätten ferrite α_W
Diffusionless nucleation Diffusionless growth	Paraequilibrium nucleation Diffusionless growth	Paraequilibrium nucleation Paraequilibrium growth

6. SIMULATION OF TTT & CCT DIAGRAMS

Assuming the applicability of classical nucleation theory, neglecting strain energy, Russell [22] obtained several expressions for calculating the time τ_s needed to reach a steady–state nucleation rate, for a variety of grain–boundary nucleation phenomena, with the general form:

$$\tau \propto \frac{T}{(\Delta G_m)^p D} \tag{12}$$

where p is an exponent which depends on the nature of the interface between the nucleus and matrix, and D is a diffusion coefficient. If τ_s is empirically identified with the incubation time τ observed for the beginning of transformation in time–temperature transformation diagrams, then it is possible to establish a reasonable method for calculating the initiation of transformation by generalising equation 12 as follows [23, 24]:

$$\ln\left\{\frac{\tau(\Delta G_m)^p}{T^z}\right\} = \frac{Q'}{RT} + C_4 \tag{13}$$

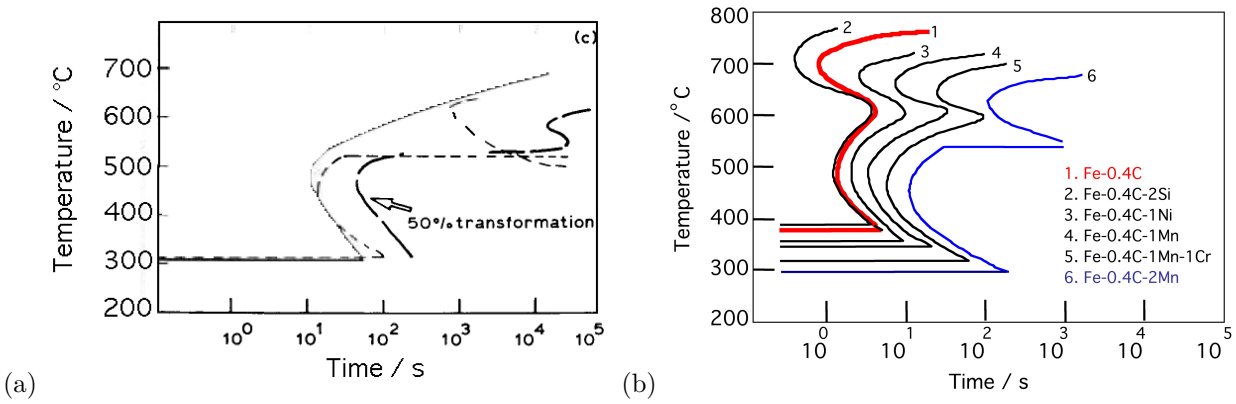

Figure 6: (a) The calculated curve shows a bay, which is incorrectly not present in the corresponding 0% transformation measured–curve, but is evident in the 50% transformation measured–curve, in the correct location. (b) An example set of TTT diagram calculations for hypothetical steels. After [23].

where Q', C_4, p and z are obtained by fitting to well–behaved experimental TTT diagrams. The method has proved extremely successful in a variety of computer programs, ranging from the design of steel weld metals, steel processing, *etc.* and is available in the public domain under the title MUCG46 [25]. The physical basis of the program is interesting in that it has identified by calculation, a number of errors in published diagrams [23]). An example of such a case is illustrated in Fig. 6a, where the bay is absent in the experimental 0% transformation curve, whereas consistent with the calculation (long dashes), there is a bay in the correct location in the 50% transformation experimental curve.

Since the original work referred to the initiation of the bainite transformation, Takahashi and Bhadeshia [26] extended it to the progress of transformation for steels in which the bainite grows without the precipitation of cementite from austenite. The method nevertheless does not account for the full panoply of theory available. A much more fundamental model has been published recently [27] – however, the comparison with experimental data is limited and intensive research is in progress to properly validate the method and indeed, to integrate the new model into the scheme of solid–state transformations in steels.

Once a TTT diagram is obtained, a variety of assumptions can be made to convert it to a continuous cooling transformation diagram. The basis for this is fully described by Christian [28]; for the sake of brevity, the methods are not reviewed here.

7. "SUPERBAINITE"

The goal of much of the research on structural nanomaterials is to obtain a strong material which can be used for making components which are large in all their dimensions, and which does not require mechanical processing or rapid cooling to reach the desired properties. The following conditions are required to achieve this [29]:

(i) The material must not rely on perfection to achieve its properties. Strength can be generated by incorporating a large number density of defects such as grain boundaries and dislocations, but the defects must not be introduced by deformation if the shape of the material is not to be limited.

(ii) Defects can be introduced by phase transformation, but to disperse them on a sufficiently fine scale requires the phase change to occur at large undercoolings (large free energy changes). Transformation at low temperatures also has the advantage that the microstructure becomes refined.

(iii) A strong material must be able to fail in a safe manner. It should be tough.

(iv) Recalescence limits the undercooling that can be achieved. Therefore, the product phase must be such that it has a small latent heat of formation and grows at a rate which allows the ready dissipation of heat.

It has long been known that lowering the transformation temperature for bainite leads to a finer structure (*e.g.* [30]). It is now known that bainite with an incredibly fine structure can be produced by phase transformations at low temperatures. Recent discoveries have shown that carbide–free bainite can satisfy these criteria [29, 31–36].

Bainite and martensite are generated from austenite without diffusion by a displacive mechanism. Not only does this lead to solute–trapping but also a huge strain energy term, both of which reduce the heat of transformation. The growth of individual plates in both of these transformations is fast, but unlike martensite, the *overall rate* of reaction is much smaller for bainite. This is because the transformation propagates by a sub–unit mechanism in which the rate is controlled by nucleation rather than growth. This mitigates recalescence.

The theory of the bainite transformation allows the estimation of the lowest temperature at which bainite can be induced to grow. There is in principle no lower limit to the temperature at which bainite can be generated. On the other hand, the rate at which bainite forms slows down dramatically as the transformation temperature is reduced. It may take hundreds or thousands of years to generate bainite at room temperature. For practical purposes, the carbon concentration has to be limited to about 1 wt%.

An alloy has been designed in this way, with the approximate composition Fe–1C–1.5Si–1.9Mn–0.25Mo–1.3Cr-0.1V wt%, which on transformation at 200°C, leads to bainite plates which are only 20–40 nm thick. The slender plates of bainite are dispersed in stable carbon–enriched austenite which, with its face–centred cubic lattice, buffers the propagation of cracks.

The "superbainite" is the hardest ever (700 HV, 2500 $\mathrm{MN\,m^{-2}}$), has considerable ductility, is tough (30-40 $\mathrm{MPa\,m^{1/2}}$) and does not require mechanical processing or rapid cooling. The steel after heat–treatment therefore does not have long–range residual stresses, it is very cheap to produce and has uniform properties in very large sections. In effect, the hard bainite has achieved all of the essential objectives of structural nanomaterials which are the subject of so much research, but in large dimensions.

8. MECHANICAL PROPERTIES

A high density of internal surfaces is not always good for a steel. This is because the boundaries either act as sinks for dislocations or there is insufficient room for dislocation multiplication mechanisms to operate. As a consequence there is no mechanism for work hardening and nanostructured materials therefore suffer from plastic instability soon after yielding [37, 38]. Indeed, in one experiment, a nanostructured ferrite when forced to shear failed to deform by ordinary mechanisms and instead underwent displacive transformation to austenite at room temperature as a way of accommodating the applied stress [39].

The motivation for ever finer grain sizes comes from a desire for stronger materials. Work–hardening must therefore be introduced into nanostructured materials to avoid plastic instabilities and hence enable the exploitation of strength. This has been achieved in a wonderful steel by introducing retained austenite between plates of bainite, each of which is thinner than a typical carbon nanotube [29, 34–36, 40–42], Fig. 7. Notice that although the thickness of the plates is of the order of 20–40 nm, their length is much longer. Nevertheless, the mean slip distance through a plate is about twice the thickness, so in spite of the anisotropy of shape, this can, from a strength point of view, be classified as a nanostructured metal. The mixture of large and small dimensions is an advantage over equiaxed grains in giving a much greater amount of surface per unit volume within the bulk [43].

In this microstructure, the austenite transforms into martensite under the influence of applied stress and this results in work hardening, with large and almost completely uniform plastic strain Fig. 8, details listed in Table . What then determines the fracture strain?

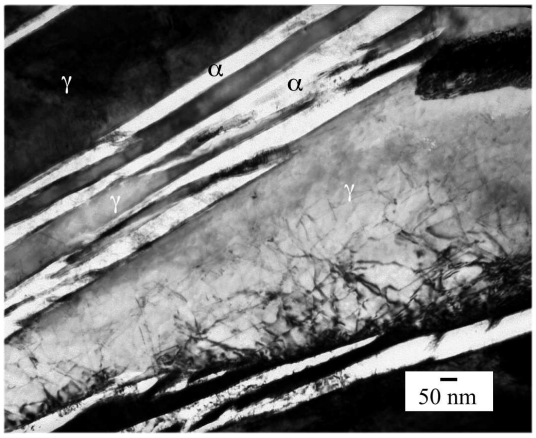

Figure 7: Fe-0.98C-1.46Si-1.89Mn-0.26Mo-1.26Cr-0.09V wt%, transformed at 200°C for 5 days. Transmission electron micrograph [35, 36, 40].

The change in the austenite content with plastic strain and the driving force for martensitic transformation can be estimated as shown in Fig. 9 for the cases listed in Table [45]. Also plotted are points which define

T_I / °C	V_γ	σ_Y / GPa	σ_{UTS} / GPa	Elongation / %
200	0.17	1.41	2.26	7.6
300	0.21	1.40	1.93	9.4
400	0.37	1.25	1.7	27.5

Table 2: T_I, V_γ, σ_Y and σ_{UTS} stand for isothermal transformation temperature, the volume fraction of retained austenite, the 0.2% proof and ultimate tensile strengths respectively [44].

in each case the strain at which the tensile samples failed. A prominent feature is that they all fail when the retained austenite content is reduced to about 10%. An experimental study by Sherif [46] on an aluminium–free alloy which is otherwise identical to the steel considered here, is consistent with this conclusion. His X–ray studies also indicated that tensile failure in nanostructured bainite occurs when the retained austenite content is diminished to about 10%.

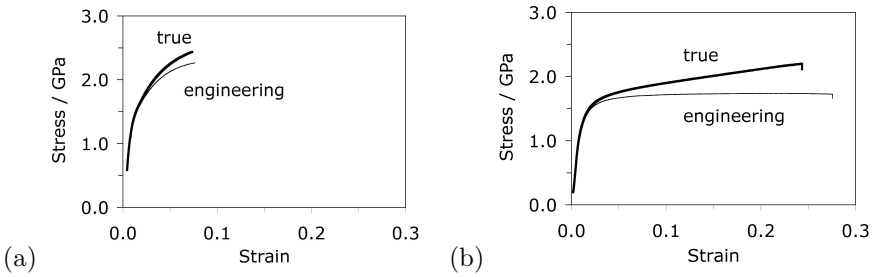

Figure 8: Fe–0.79C–1.56Si–1.98Mn–0.24Mo–1.01Cr–1.51Co–1.01Al wt%. True and engineering stress–strain curves. (a) Bainite generated by transformation at 200°C. (b) Bainite generated by transformation at 300°C. Data from [44].

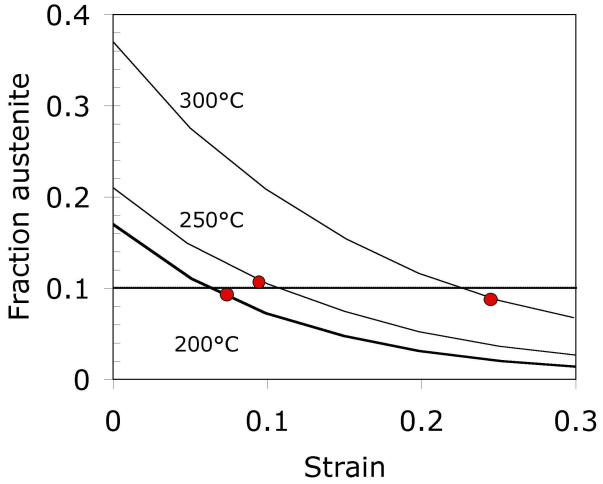

Figure 9: Calculated variation in the fraction of austenite as a function of plastic strain for the samples listed in Table 2. Also marked are points indicating the measured fracture strain for each case. Fracture seems to occur when the austenite content decreases to about 10% of the microstructure. Data adapted from [44].

This observation can be understood if it is assumed that failure occurs when the austenite, which is the toughest of all the phases present, becomes geometrically isolated, *i.e.,* it loses percolation, leading to fracture. Garboczi *et al.* have developed a numerical model for the percolation threshold when freely overlapping objects (general ellipsoids) are placed in a matrix [47]. Since the austenite is subdivided roughly into the form of plates by the bainite, it can be represented by oblate ellipsoids with an aspect ratio r of between about 1/10 and 1/100. The percolation threshold is then found to be $p_c \simeq 1.27r$, *i.e.,* $0.127 \geq p_c \geq 0.0127$. This is consistent with the observation that tensile failure occurs when $V_\gamma \simeq 0.1$.

It seems then that the formation of hard, stress/strain–induced martensite can only be tolerated if the austenite maintains a continuous path through the test sample.

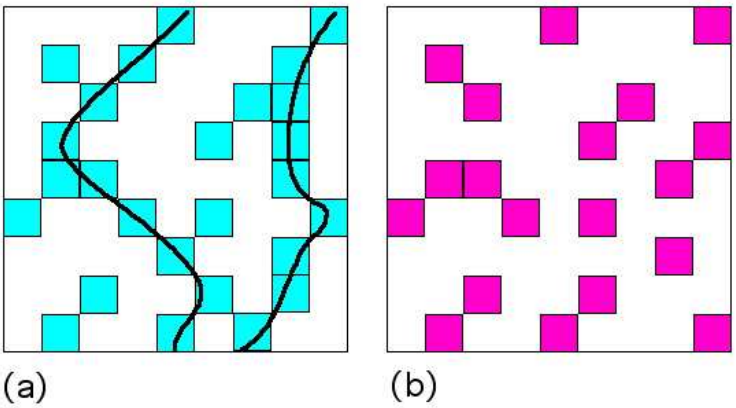

Figure 10: An illustration of percolation. In (a) the coloured phase has a fraction beyond the percolation threshold and in (b) it is below that threshold.

9. SUMMARY

The future looks good for carbide–free bainitic steels, which are now well understood both with respect to the atomic mechanism of transformation and the mechanical behaviour of its composite microstructures. One outstanding problem is a quantitative theory for the influence of elements such as silicon which inhibit cementite precipitation from austenite.

References

[1] M. F. Ashby: Materials Selection in Mechanical Design: Pergamon Press, Oxford, U. K., 1993.

[2] H. K. D. H. Bhadeshia: Acta Metallurgica 29 (1981) 1117–1130.

[3] H. K. D. H. Bhadeshia: Bainite in Steels, 2nd edition: Institute of Materials, London, 2001.

[4] A. Ali, H. K. D. H. Bhadeshia: Materials Science and Technology 6 (1990) 781–784.

[5] H. K. D. H. Bhadeshia: Materials Science and Technology 1 (1985) 497–504.

[6] H. K. D. H. Bhadeshia: Metal Science 15 (1981) 175–177.

[7] H. K. D. H. Bhadeshia: Metal Science 15 (1981) 178–150.

[8] Y. Imai, M. Izumiyama, M. Tsuchiya: Scientific Reports: Research Institute of Tohoku University A17 (1965) 173–192.

[9] L. Kaufman, M. Cohen: Progress in Metal Physics 7 (1958) 165–246.

[10] G. Ghosh, G. B. Olson: Journal of Phase Equilibria 22 (2001) 199–207.

[11] C. G. Mateo, H. K. D. H. Bhadeshia: Materials Science and Engineering A 378A (2004) 289–292.

[12] J. W. Christian: Proceedings of the Royal Society of London A 206A (1951) 51–64.

[13] G. B. Olson, M. Cohen: Metallurgical Transactions A 7A (1976) 1897–1923.

[14] H. Conrad: Journal of Metals July (1964) 582–588.

[15] J. E. Dorn: Low temperature dislocation mechanisms: in: A. R. Rosenfield, G. T. Hahn, A. L. Bement, R. I. Jaffee (Eds.), Dislocation dynamics: McGraw Hill, New York, 1968: p. 27.

[16] G. B. Olson, H. K. D. H. Bhadeshia, M. Cohen: Acta Metallurgica 37 (1989) 381–389.

[17] H. K. D. H. Bhadeshia: Solute–drag, kinetics and the mechanism of the bainite transformation: in: A. R. Marder, J. I. Goldstein (Eds.), Phase Transformations in Ferrous Alloys: TMS–AIME, Ohio, USA, 1984: pp. 335–340.

[18] H. K. D. H. Bhadeshia, J. W. Christian: Metallurgical & Materials Transactions A 21A (1990) 767–797.

[19] H. K. D. H. Bhadeshia, D. V. Edmonds: Acta Metallurgica 28 (1980) 1265–1273.

[20] J. W. Christian: Theory of Transformations in Metal and Alloys, Part II: 3rd Edition: Pergamon Press, 2003.

[21] R. F. Hehemann: The bainite transformation: in: H. I. Aaronson, V. F. Zackay (Eds.), Phase Transformations: 1970: pp. 397–432.

[22] K. C. Russell: Acta Metallurgica 16 (1968) 761–769.

[23] H. K. D. H. Bhadeshia: Metal Science 16 (1982) 159–165.

[24] J. L. Lee, H. K. D. H. Bhadeshia: Materials Science and Engineering A A171 (1993) 223–230.

[25] U. of Cambridge, NPL: Materials Algorithms Project, www.msm.cam.ac.uk/map/mapmain.html. URL `www.msm.cam.ac.uk/map/mapmain.html`

[26] M. Takahashi, H. K. D. H. Bhadeshia: Materials Transactions JIM 32 (1991) 689–696.

[27] H. Matsuda, H. K. D. H. Bhadeshia: Proceedings of the Royal Society of London A A460 (2004) 1710–1722.

[28] J. W. Christian: Theory of Transformations in Metal and Alloys, Part I: 3rd Edition: Pergamon Press, Oxford, U. K., 2003.

[29] H. K. D. H. Bhadeshia: Materials Science and Technology 21 (2005) 1293–1302.

[30] S. B. Singh, H. K. D. H. Bhadeshia: Materials Science and Engineering A A245 (1998) 72–79.

[31] F. G. Caballero, H. K. D. H. Bhadeshia, K. J. A. Mawella, D. G. Jones, P. Brown: Materials Science and Technology 17 (2001) 512–516.

[32] F. G. Caballero, H. K. D. H. Bhadeshia, K. J. A. Mawella, D. G. Jones, P. Brown: Materials Science and Technology 17 (2001) 517–522.

[33] C. Garcia-Mateo, F. G. Caballero, H. K. D. H. Bhadeshia: ISIJ International 43 (2003) 1238–1243.

[34] C. Garcia-Mateo, F. G. Caballero, H. K. D. H. Bhadeshia: ISIJ International 43 (2003) 1821–1825.

[35] F. G. Caballero, H. K. D. H. Bhadeshia: Current Opinion in Solid State and Materials Science 8 (2005) 186–193.

[36] F. G. Caballero, H. K. D. H. Bhadeshia, K. J. A. Mawella, D. G. Jones, P. Brown: Materials Science and Technology 18 (2002) 279–284.

[37] A. A. Howe: Materials Science and Technology 16 (2000) 1264–1266.

[38] N. Tsuji, Y. Ito, Y. Saito, Y. Minamino: Scripta Materialia 47 (2002) 893–899.

[39] Y. Ivanisenko, I. MacLaren, R. Z. Valiev, H. J. Fecht: Advanced Engineering Materials 7 (2005) 1011–1014.

[40] C. Garcia-Mateo, F. G. Caballero, H. K. D. H. Bhadeshia: Journal de Physique Colloque 112 (2003) 285–288.

[41] M. Peet, S. S. Babu, M. K. Miller, H. K. D. H. Bhadeshia: Scripta Materialia 50 (2004) 1277–1281.

[42] M. Peet, C. Garcia-Mateo, F. G. Caballero, H. K. D. H. Bhadeshia: Materials Science and Technology 20 (2004) 814–818.

[43] C. Mack: Proceedings of the Cambridge Philosophical Society 52 (1956) 286.

[44] C. Garcia-Mateo, F. G. Caballero: Materials Transactions 46 (2005) 1839–1846.

[45] M. Sherif, C. Garcia-Mateo, T. Sourmail, H. K. D. H. Bhadeshia: Materials Science and Technology 20 (2004) 319–322.

[46] M. Y. Sherif: Characterisation and development of nanostructured, ultrahigh strength, and ductile bainitic steels: University of Cambridge, 2005.

[47] E. J. Garboczi, K. A. Snyder, J. F. Douglas, M. F. Thorpe: Physical Review E 52 (1995) 819–828.